SPARC-BD-03/005
28 July 2003

STATUS OF THE LOW-ENERGY EMITTANCE MEASUREMENT SIMULATIONS FOR THE SPARC PROJECT

M. Boscolo[1], A. Cianchi[2], M. Ferrario[1], L. Picardi[3], M. Quattromini[3], C. Ronsivalle[3], J. Rosenzweig[4]

[1] *INFN-LNF*

[2] *University of Roma "Tor Vergata"*

[3] *ENEA-Frascati*

[4] *UCLA*

Abstract

The commissioning phase of the SPARC RF-gun foresees the measure of the beam emittance in the post RF-gun region where the process of emittance compensation occurs. The space charge dominated beam evolution does not allow the use of the quad-scan method; so an array of narrow slits separating the beam into several beam-lets whose intensity distribution will be collected from a view-screen at a downstream point will be used. From the analysis of the beamlet size and position the beam phase space will be retrieved.

We developed a numerical simulation of this type of measure based on PARMELA and TREDI simulations that can be a useful tool to evaluate the achievable accuracy and to optimize the experimental setup. In this paper the results of this activity are presented.

1 INTRODUCTION

The first phase of the SPARC Project consists of the commissioning of the photocatode RF gun (5.6 MeV beam). It foresees the systematic emittance measurement along the post-RF gun drift where the emittance compensation process occurs. For this measurement a dedicated movable (in z) emittance measurement tool will be used giving the possibility to perform measurements from z=85 cm to z=200 cm (the cathode is at z=0).
The technique that will be employed for the emittance measurement consists in selecting one or several sample beam-lets by means of an intercepting multi-slit mask (fig.1) or a single slit moving over the beam spot. The slits reduces the space charge dominated incoming beam into some emittance-dominated beam-lets that drift up to an intercepting screen. The intensity of beam-let spots on the screen is directly proportional to the number of particles in the beam-lets which hit the screen and the rms un-normalized emittance value can be retrieved by the formula reported in appendix 1, derived from ref. [1], that employs only geometrical parameters of the slits and of the spots on the screen.

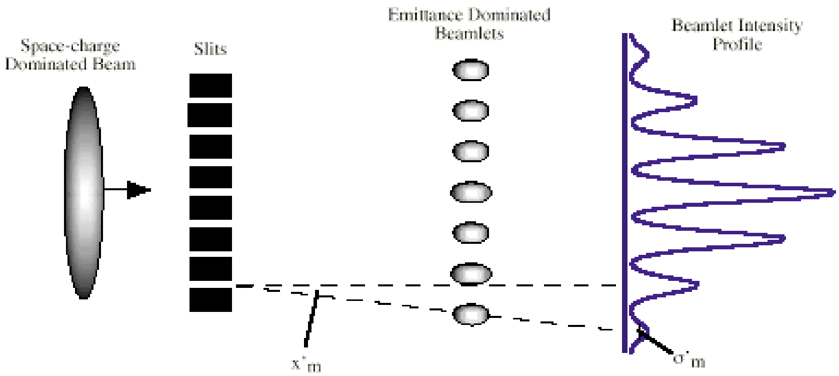

Figure 1: Multi-slit – based emittance measurement scheme

Analytical considerations based on the envelope equation (see appendix 2 and ref [2]) applied to the SPARC beam (I□100 A, □□0.5 mm, $□_{msn}$ □ 1 mm mrad) yield to a slit width d< 66 □m in order to have an emittance - dominated beam expansion. The slit spacing *w* has to be chosen much larger than the slit width and smaller than the beam size to ensure that the beam can be resolved (d<*w*< □).
The drift length L between the slit plate and the output screen is a compromise between two requests: it has to be big enough to have a high resolution for the low beam emittance, but small enough to prevent the overlapping of the beam-let profiles on the screen.
Numerical simulations of such a measure, based on PARMELA beam dynamics calculation, have been done in order to optimise the main mechanical measurement assembly parameters, to evaluate the effect of the residual space charge, to evaluate the maximum accuracy that can be reachable in the whole z range of interest and to compare the use of a single-shot multi-slit measurement with the use of a multi-shot moving single slit measurement.
In this paper we report the preliminary results of this activity.

2 THE "VIRTUAL" MEASUREMENT

The first step of the numerical simulation of the emittance measurement is the beam dynamics calculation in the SPARC region gun + drift. The plot of fig.2 shows the normalized rms emittance and rms x-envelope computed by PARMELA in this region. The temporal distribution of the 1 nC input beam is given by a pulse with a 11.7 psec width (FWHM) and 1 psec rise time simulated in PARMELA by stacking 15 gaussians, while the radial distribution is uniform. The thermal emittance is about 0.3 mm mrad. The gun peak electric field is 120 MV/m and the magnetic field

produced by the emittance compensating solenoid is 2.73 Kgauss. This set of parameters minimizes the beam emittance at the output of the accelerating sections (0.6 mm mrad).. The particles coordinates are saved in a binary file along the drift at steps of 5 cm in order to have the possibility to introduce in different points of the drift an intercepting multislit mask, simulated by cutting the output PARMELA distribution with a post-processor. The surviving particles are traced in a successive PARMELA run from the "cutting" point (the mask plane) up to the output screen.
Usually 15K particles are sufficient to get stable results, but for the simulation of the emittance measurement we started from 450K particles, in order to have, after the cut, a number of particles that can be sufficient for the successive computation that requires a large number of particles (50K at least), if one wants to take into account the residual space charge effect (3D calculation is needed being the beamlets a collection of sheet beams).

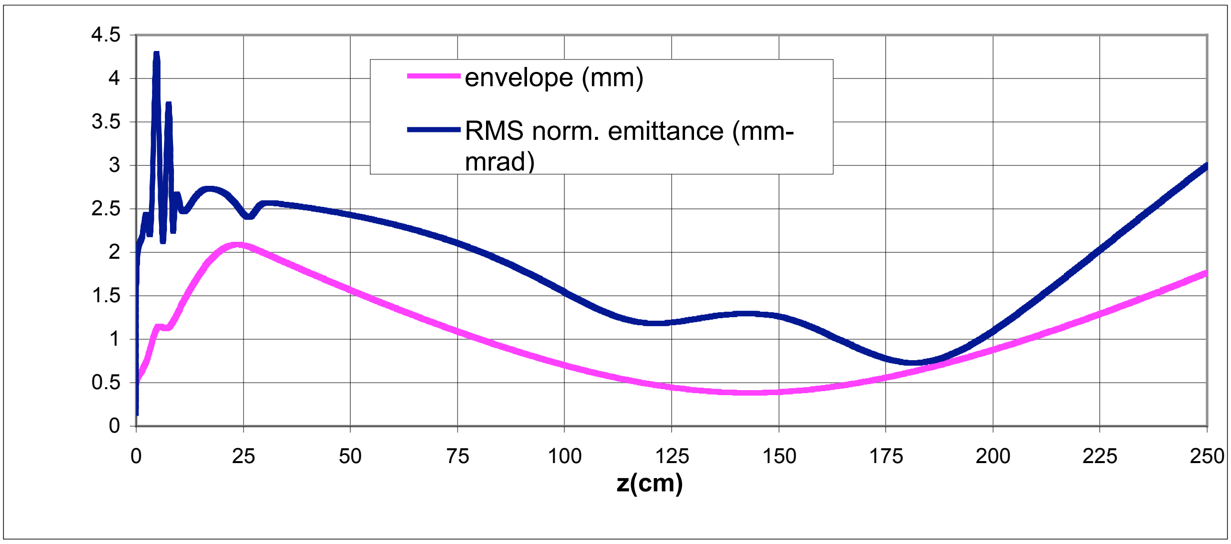

Figure: 2 -RMS normalized emittance and RMS x-envelope in the gun+drift region computed by PARMELA

A MATLAB-based program generates a realistic output image on a tiff file from of a density plot of the particles distribution on the output screen, computed by PARMELA. The tiff file data can be thus analysed by the data acquisition programs used by the SPARC diagnostic team to extract the emittance value from the intensity distribution.
However in order to check the consistency of the method and to have a preliminary evaluation of the possible errors due to different types of effects (evolution of the beam phase space along the drift, residual space charge, emittance filtering action of the non-zero thickness of the mask plate, centroid displacement) we wrote also an analysis MATLAB-based program which through a simplified algorithm retrieves the phase-space parameters from the tiff file where the simulated image has been recorded and gives the possibility to compare the PARMELA value of the emittance with the emittance value that can be retrieved from the "virtual" measure.
The algorithm separates the output distribution peaks of the single beamlets identifying the minima between the peaks and then retrieves the mean position and the mean divergence of all beamlets.
A typical sequence of this procedure is shown in figures 3,4 and 5.

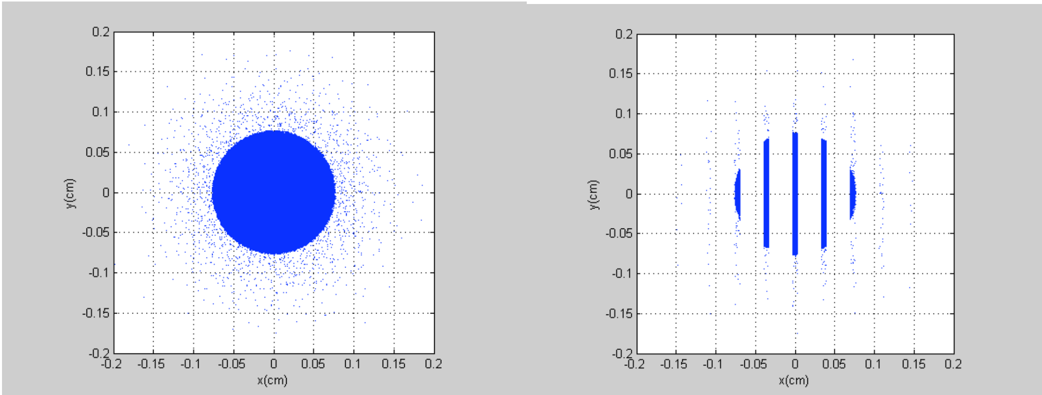

Figure 3: xy plot of PARMELA distribution at z=150 cm before the slits (Np=450K) and immediately after a zero thickness multi slit plate with d=65 μm, w = 300 μm (Np=74671)

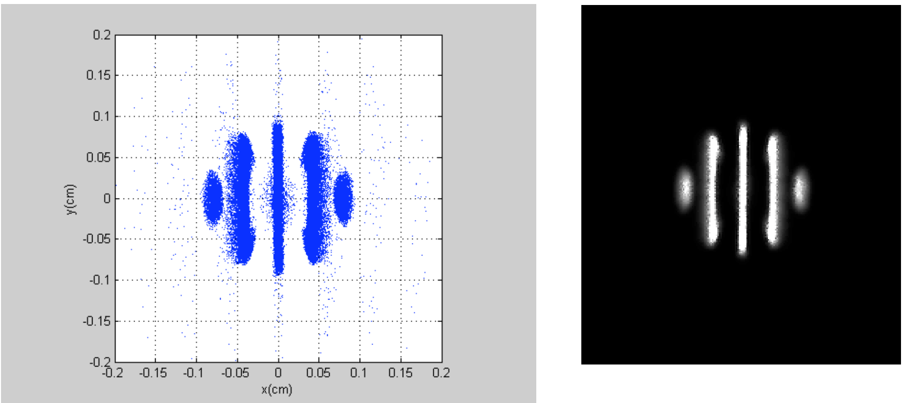

Figure. 4: xy plot of PARMELA distribution at z=170 cm and the relative reconstructed image on the output screen

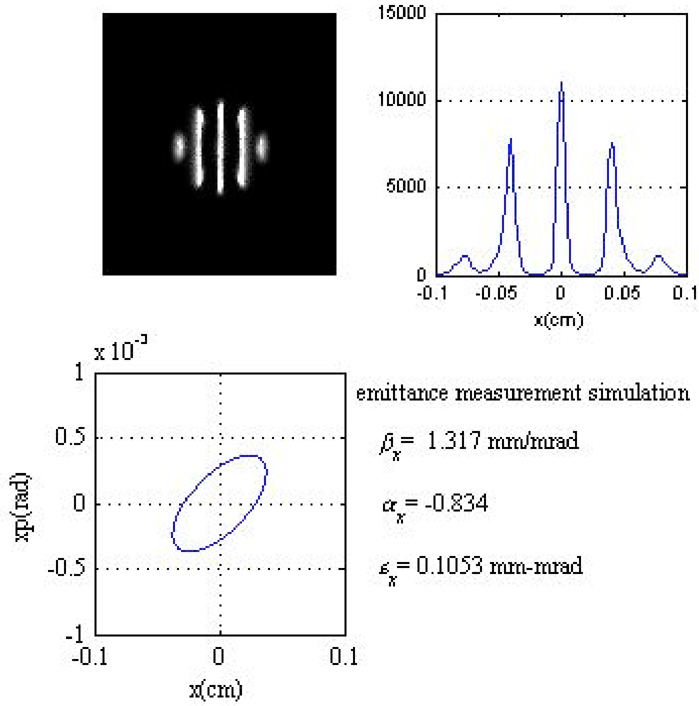

Figure 5: Output of the MATLAB program analysing the PARMELA distribution on the output screen(L=20 cm)

3 MASK THICKNESS EFFECT

The case shown in the figures 3,4 and 5 of the previous paragraph correspond to an “ideal” zero thickness multi-slit plate. The choice of the thickness of the real plate is dictated by the need to either stop the beam or scatter it sufficiently so that it does not affect the measurement of non intercepted beam-lets. In our case 2 mm of tungsten could stop the beam because this depth corresponds to the “range” of 5.6 MeV electrons in tungsten (fig.6). The finite angular acceptance of the slit plate due to the plate thickness and the slits dimension works as an emittance filter, resulting in an under-estimation of the emittance. This error has been evaluated in the whole z range of our measurement for two different values of slit width, 25 and 50 μm (a distance between the centres of the slits of 500 μm is assumed). Of course due to the different dimensions and angles of the envelope (as it can be seen in fig.2) this error is minimum in the waist region and maximum where the beam is strongly converging or diverging, i.e. at the ends of the region covered by the movable emittance measurement tool.

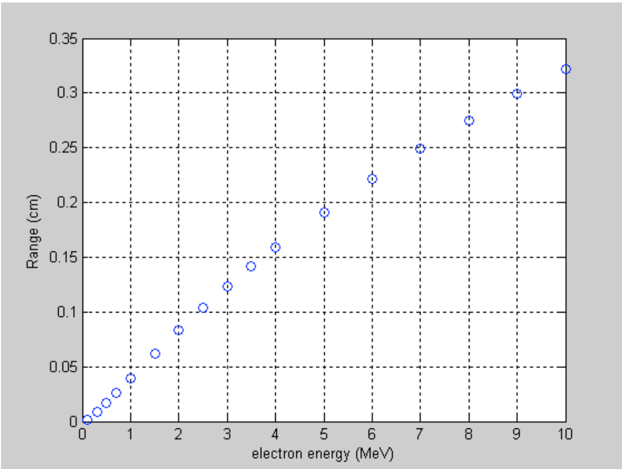

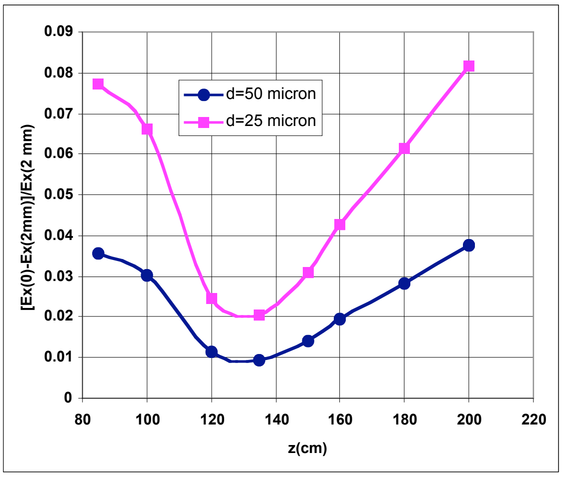

Figure 6: Electron range in tungsten vs energy (data from NIST database) , Fig. 7 Emittance error due to the acceptance of the slit plate for a plate thickness of 2 mm and two values of the slit width.

The calculation results that will be reported in the rest of this paper refer to a 2 mm thick plate in which the fractional loss of particles due to the angular acceptance of the slits is taken into account. At the moment only this emittance-filter effect produced by the finite thickness of the mask has been considered. No calculations have been done to evaluate how the measure is affected by the noise produced by the slit scattering. Montecarlo calculations based on EGS4 code reported in Ref. [3] for a well-aligned pepper-pot and a 8 MeV beam indicate that this effect is negligible, but however we plan to include also this effect in our simulations.

4 EFFECTS OF THE DIFFERENT BEAM PHASE SPACE

In the emittance compensation region where the emittance will be measured the beam characteristics in terms of emittance and envelope (see fig. 2 paragraph 2) change largely so we can expect that an optimisation study will require different parameters for the emittance-meter in order to maximise the accuracy everywhere. So we divided the measure region extending from 85 cm to 200 cm (z=0 at the cathode) in 3 sub-regions characterized by a different behaviour of the beam: the converging beam region, the waist region and the diverging region and we analysed the problems connected to the measurement separately in each sub-region. In the following analysis we used a slit width of 50 μm and a distance between the centres of the slits of 500 μm that are within machining capabilities and a plate thickness of 2 mm. In this paragraph only the effect of the shape of the envelope in the drift will be considered (space charge is switched off after the mask) while the effect of the residual space charge will be treated in the paragraph 5.

4.1 The converging beam region

This region extends approximately from z=85 cm to z=120 cm. In figure 8 the x-x' phase space plots as computed by PARMELA are shown.

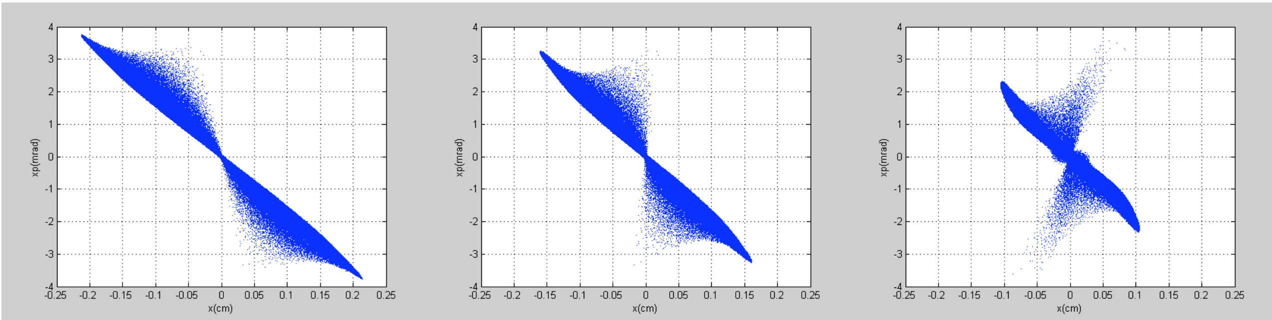

Figure 8: PARMELA output x'-x plots in 3 z locations: from left to right z=85 cm, z=100 cm, z=120 cm

In this region the main problem is given by the rapid overlap of the beamlets with the increasing of the distance between the intercepting mask and the output screen , as it can be observed in figure 9 where the intensity plot on the output screen is shown for a mask placed at z=1 m and four different positions of the output screen (L=10,20,30,40 cm).

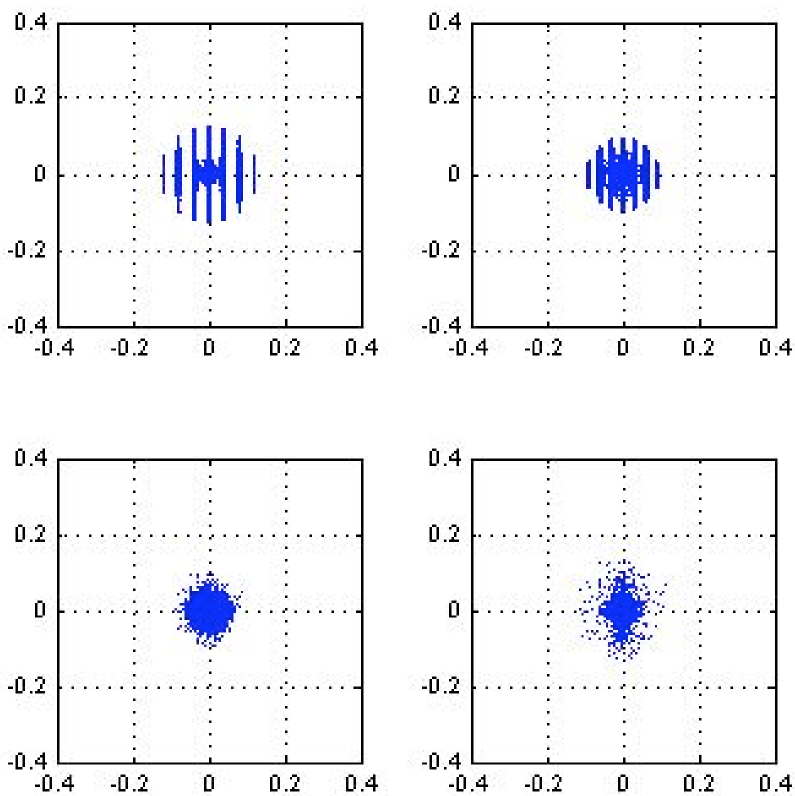

Figure 9: From left to right and from top to bottom the intensity plot on output screen for L=10,20,30,40 cm. The multi-slit mask is placed at z=1 m.

4.2 The waist region

This region extends approximately from z=120 cm to z=160 cm. In figure 10 the x-x’ phase space plots as computed by PARMELA are shown.

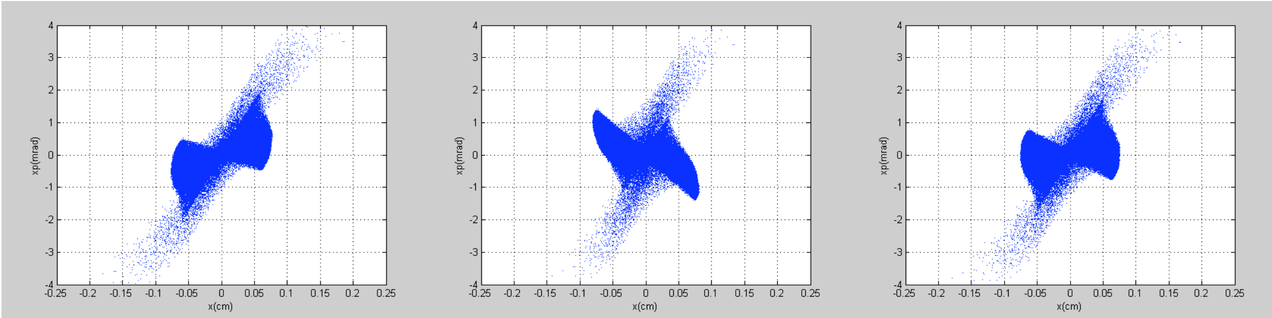

Figure 10: PARMELA output x’-x plots in 3 z locations: from left to right z=135 cm, z=145 cm, z=150 cm

Due to the small beam size, the waist region requires a fine sampling, as it is shown in fig. 11 where the PARMELA un-normalized rms emittance values are compared with the emittance values that can be retrieved from the simulated measurement for two different sets of parameters. Around z=1.3 m the error drops from about 20% to about 4% passing from a multi-slit plate with d=65 μm and w=300 μm to a multi-slit plate with d=50 μm and w=450 μm.

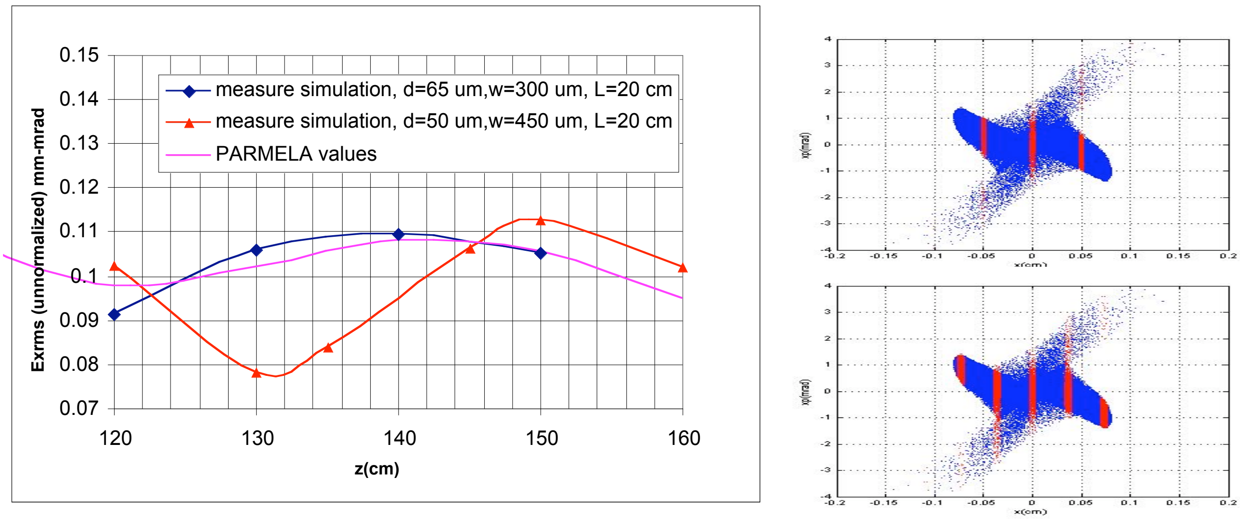

Figure 11: Comparison of the PARMELA values and retrieved emittance values (left plot) in the waist region for two different beam sampling (right plots)

4.3 The diverging beam region

This region extends approximately from z=160 cm to z=200 cm. In figure 12 the x-x’ phase space plots as computed by PARMELA are shown.
In this case (fig.13) because of the beam dimension and the fact that the beam is diverging, the use of a multi-slit method seems to be applicable because there are no problems of beam-lets overlapping or beam size resolution. In this case an adequate resolution of the angular spread of the beam requires a mask-screen distance of 40 cm at least.

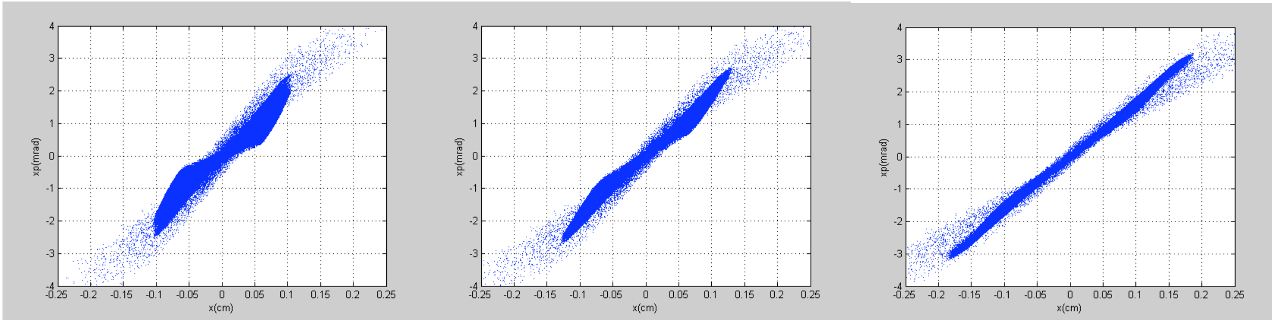

Figure 12: PARMELA output x'-x plots in 3 z locations: from left to right z=170 cm, z=180 cm, z=200 cm

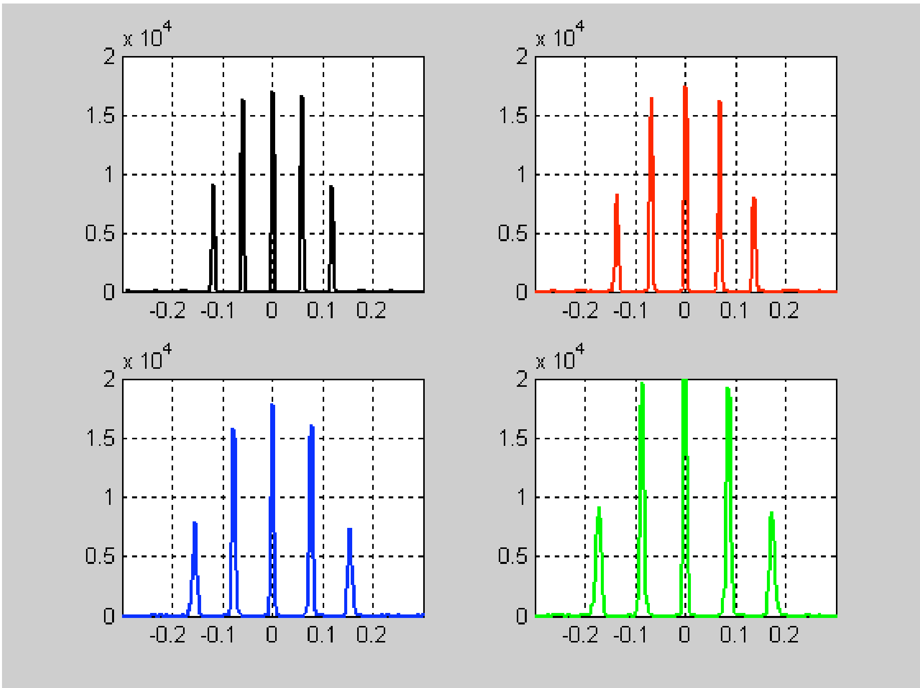

Figure 13: Ouput peaks for different for L(multislit plate-output screen distance)=10,20,30,40 cm

5 AN ALTERNATIVE METHOD TO INCREASE THE RESOLUTION

From the pervious results it seems that the application of the single-shot multislit measure appears problematic both in the region where the beam is converging due to beamlets overlapping problems and in the waist region where the beam size is small and resolution problems arise. In particular in the waist position the error drops from about 20% to about 4% reducing the distance between the centres of the slits from 500 μm (only 3 beamlets) to 250 μm (7 beamlets) . But actually it seems difficult to machining the slits with sufficient precision with such small distance. So the solution that is usually proposed to overcome this problem is the use of a single slit moving over the beam spot. The drawback in this case is the jitter coming from a multi-shot measurement (at least 7 shots are necessary). In fact fluctuations of the drive laser energy, dimensions and uniformity may cause shot-to-shot fluctuations in the beam size and emittance both directly and indirectly (by changing both the emittance compensation process and the amount of charge present in the region of measurement).

An alternative solution that could reduce the jitter effect of a multi-shot measurement is to perform a two-shots measurement by using two multi-slit plates with the same slit separation (500 μm between the slit centres) but with the slits in alternate position as it is shown in figure 14: in two measurements we can obtain the same resolution reachable in 7 independent measurements without additional fabrication problems.

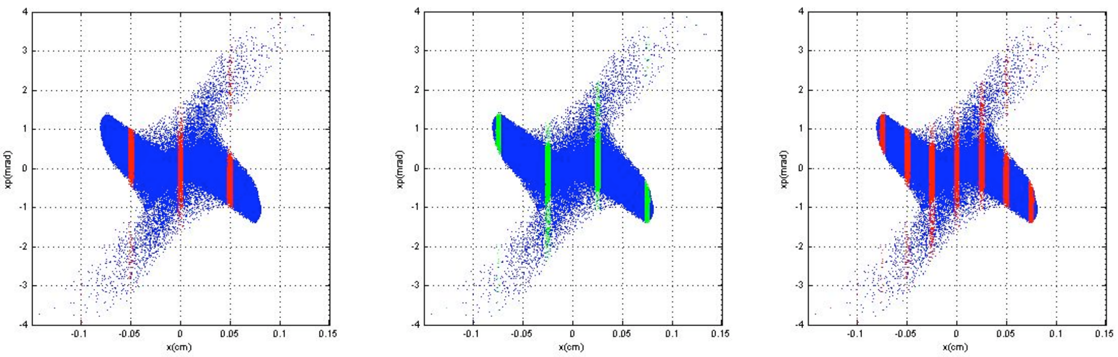

(a) **(b)** **(c)**

Figure 14: (a) the waist beam phase space covered by the multislit plate #1 (d=50μm, w+d=500μm) , (b) the waist beam phase space covered by the multislit plate #2 (d=50μm, w+d=500μm), (c) the waist beam phase space covered by 7 slits with d=50μm, w+d=250μm

6 RESIDUAL SPACE CHARGE EFFECT

Reducing the high charge beam to several beam-lets with lower charge mitigates the space charge forces. In order to evaluate the effect of the residual space charge in the region between the intercepting mask and the output screen the dynamics of a single beam-let starting from place when the emittance is minimum for two different slit widths was computed by PARMELA. Fig. 15 shows the envelope of the beam-let with the space charge on and off.

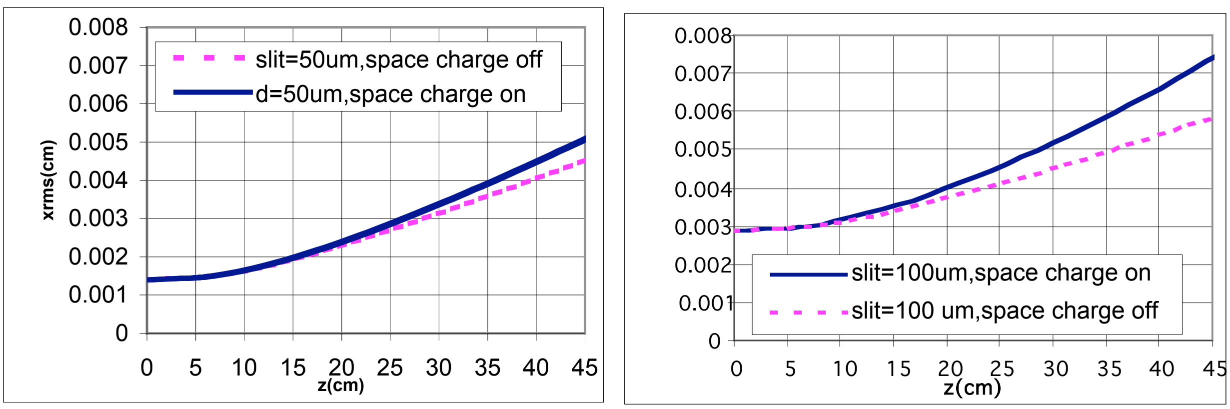

Figure 15: Expansion of a pencil beam envelope in the drift region after the mask with and without space charge for an initial beam size of 50 μm and 100 μm.

Of course reducing the beam-let size reduces the effect of the space charge. In figure 16 the percentage difference in the two examined cases is shown and one can see that for a distance less than 25 cm this difference remains under 6%.

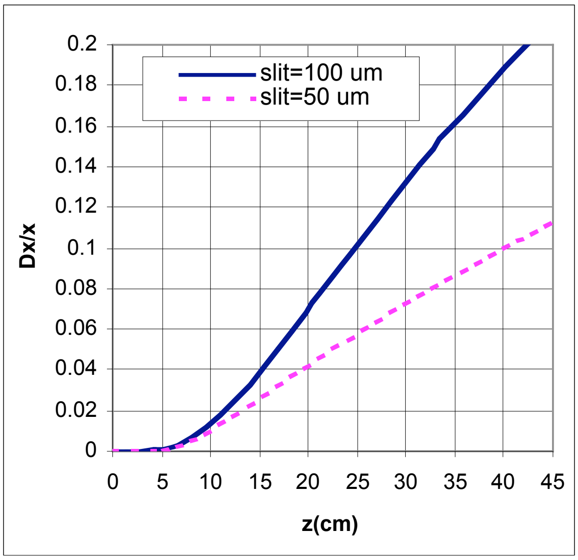

Figure 16: Percentage difference in rms beam size between the case with space charge on and the case with space charge off for a slit width of 50 μm and 100 μm

About the effect on the value of the measured emittance, we have to consider that the error should be less than this value being the horizontal distribution not uniform (fig. 17b), so that the effect for the lateral single beam-lets is reduced.

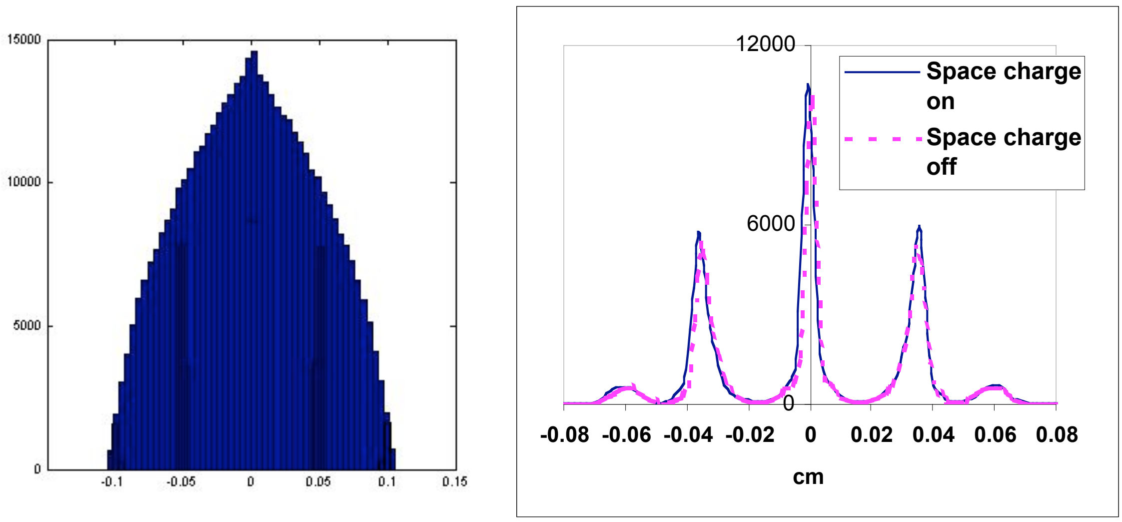

(a) **(b)**

Figure 17: (a) Horizontal distribution, (b) Computed intensity distribution on the output screen with space charge on and off

In figure 17b the intensity output screen distribution for a beam starting from the point where the emittance is minimum (z=120 mm) is compared for the case with and without space charge and it is hard to distinguish the two situations: the increase of measured emittance due to space charge is only about 2%.

7 CENTROID DISPLACEMENT EFFECT

A laser pointing instability can cause beam misalignments. The effect of a centroid displacement of 100 μm was studied in the position where the spot size is minimum. It results in an asymmetric intensity distribution on the output screen (fig.18).
The error in the measurement emittance depends from the sampling as it is shown in table 1.

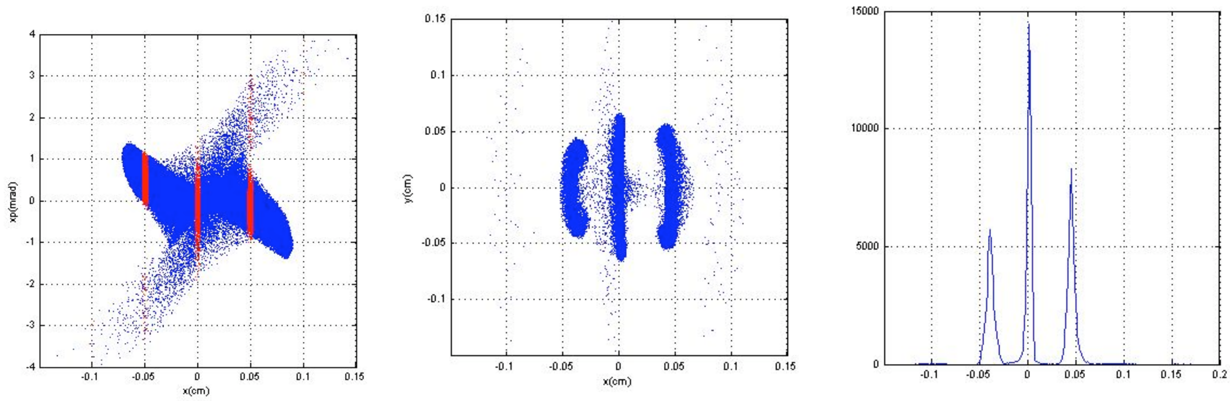

(a) **(b)** **(c)**

Figure 18: Centroid displacement=100 μm: (a) x-x' phase space + multislit with d=50 μm, w+d=500 μm, (b) x-y plot on output screen, (c) intensity distribution on output screen

TABLE 1

d+w (μm)	ε(*offset=100μm*)/ ε(*offset=0*)
500	10%
250	8%
100	1%

8 EVOLUTION OF THE RADIAL DISTRIBUTION

In fig. 19 the evolution of the horizontal and radial distribution as computed by PARMELA is shown. One can see that moving downstream from the cathode the initial uniform radial distribution tends to a hollow distribution.
This non-uniformity does not concern the whole beam, but only the central slices whose motion is dominated by space-charge as it appears in figs 20a and 20b where the distribution of an end slice and a central slice are compared soon after the waist, having divided the bunch in 10 longitudinal slices. In fact the transverse space-charge forces drop dramatically in the longitudinal "tail" regions and the particles in these slices do not focus to space-charge dominated waists, but some of them cross the axis. Viceversa the core of the bunch is dominated by space-charge and the nonlinearities of the space-charge field at the edge of the beam can drive the formation of a hollow distribution. This effect tends to reduce when the magnetic field strength is reduced as it is shown in figure 21 in which we can observe a comparison with the case of a magnetic field of B=2.66 Kgauss.

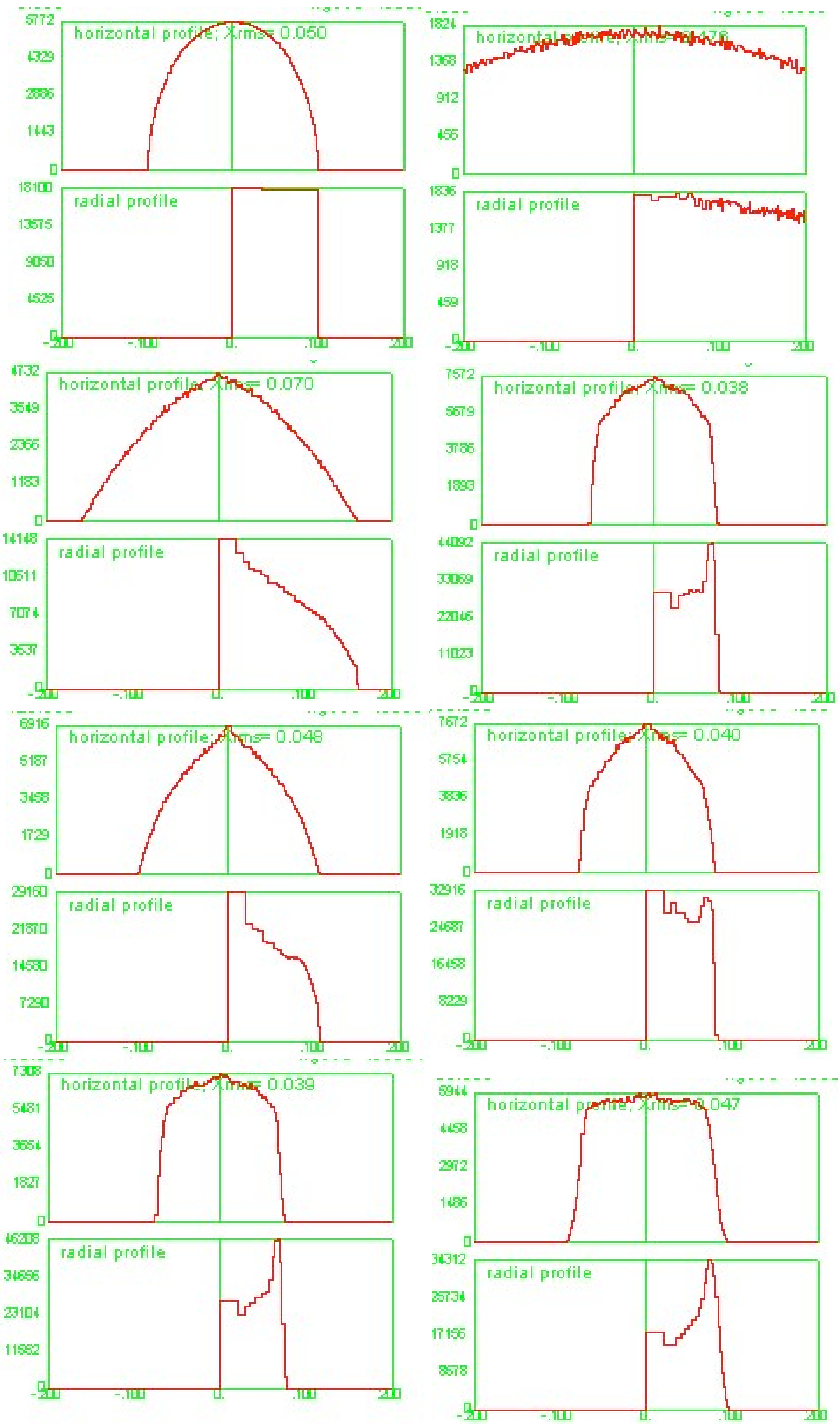

Figure 19: PARMELA output plots of horizontal and radial distribution in different longitudinal positions. First row: z=0, z=15 cm, second row: z=100, z=120 cm, third row: z=135 cm, z=145 cm, fourth row: z=150 cm, z=165 cm

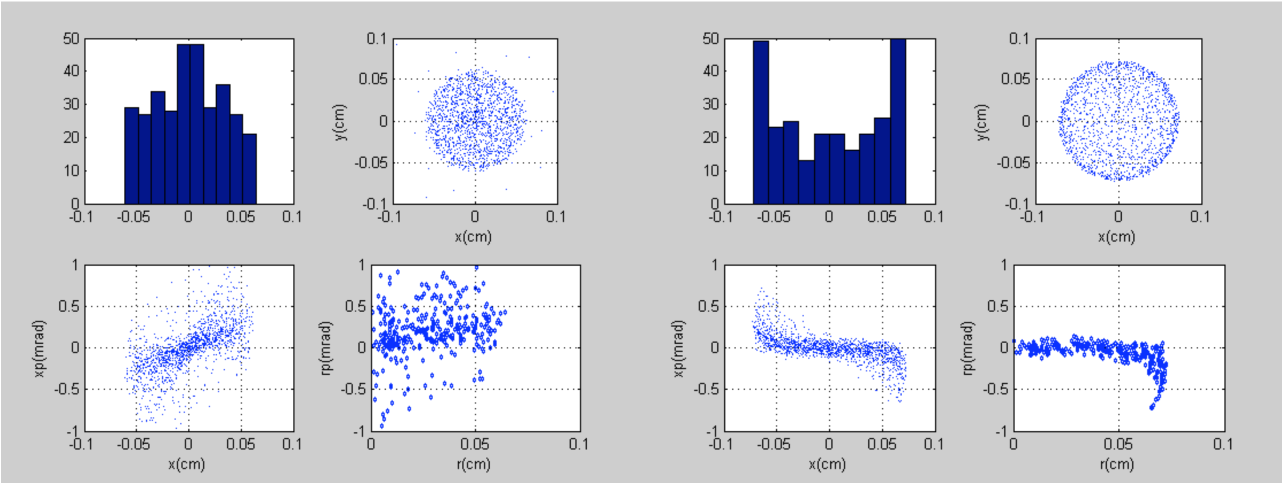

(a) (b)

Figure 20: Rad ial distribution, beam spot, x-x' space, r'-r space: (a) slice #1, (b) slice #5

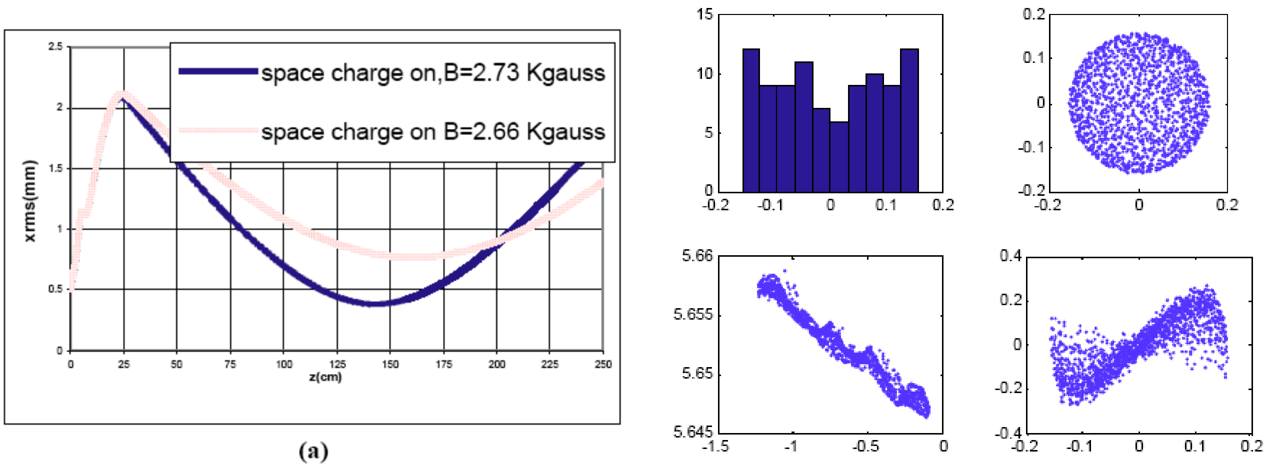

(a)

(b)

Figure 21: (a) SPARC rms horizontal envelope for B=2.73 Kgauss and B=2.66 Kgauss, (b) B=2.66 Kgauss, slice #5: radial distribution, beam spot, x-x' space, r'-r space

It is difficult at the moment to estimate in which measure these edges non-linearities could be enhanced by the numerical space-charge algorithm. In any case the acquisition system could be ready to handle this situation.

9 TREDI SIMULATIONS

A parallel analysis, has been performed by means of the TREDI simulation code, with the same set of parameters as for the PARMELA case, apart for a smaller number of particles (50K) and a different set of tools. Much like above, the beam particles tracked to a given position in the ~1.5 drift region downstream the RF gun are imported in the TREDI graphic analysis tool (written in Mathematica), where the multi slit mask is applied. The emerging particles are then stuffed back to the code, where the simulation is continued and space charge effects accounted for in "point-to-point" mode. In fact, since the beamlets surviving the selection do not possess any particular symmetry, the classical approach based on evaluation of self-fields by interpolation of the values computed on a cylindrical mesh is not suitable. Moreover, the sharp edges in the charge distribution (see fig. 22) make not advisable resorting to a 3D cartesian mesh instead, for the number of grid points required to reproduce faithfully the self-fields behaviour turns to be of the same order of magnitude as the number of particles used in the simulation.

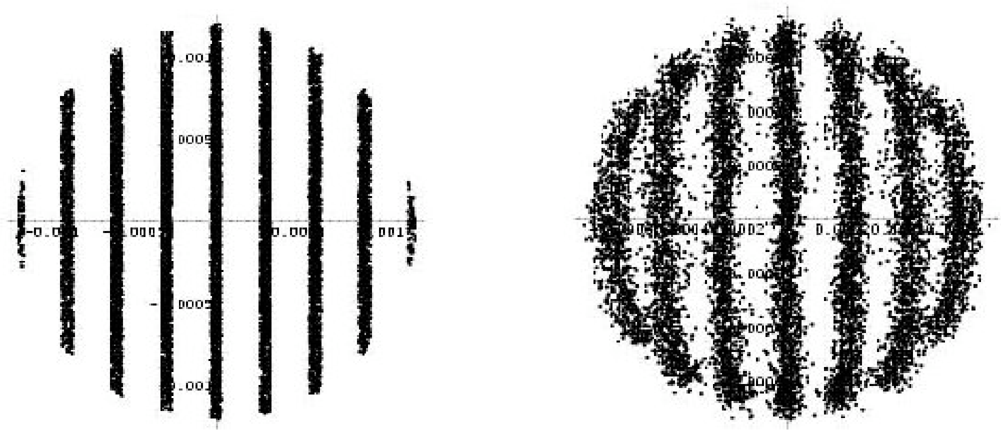

(a) **(b)**

Figure 22: (a) TREDI xy space at z=1.26m and (b) 30cm downward. The simulation was made with N=5·10^4 particles up to the slit, where a purely geometric cut has been applied. The simulation is then continued with the ~11k particles surviving the cut for 30. Self fields effects are accounted for by means of a particles-to-particles basis.

A first question is whether the self-fields play a role or not. A glimpse to the envelope (σ_x) and emittance (ε_x) plots (fig. 23(a) and (b), respectively) for a simulation made assuming the multi-slit to be placed at z=1.26m do not show any substantial difference between the evolution of the beamlets with or without space charge. This is almost always true except perhaps at the waist (z=1.50m, see figs 24a,b) where the effect of space charge is more intense.

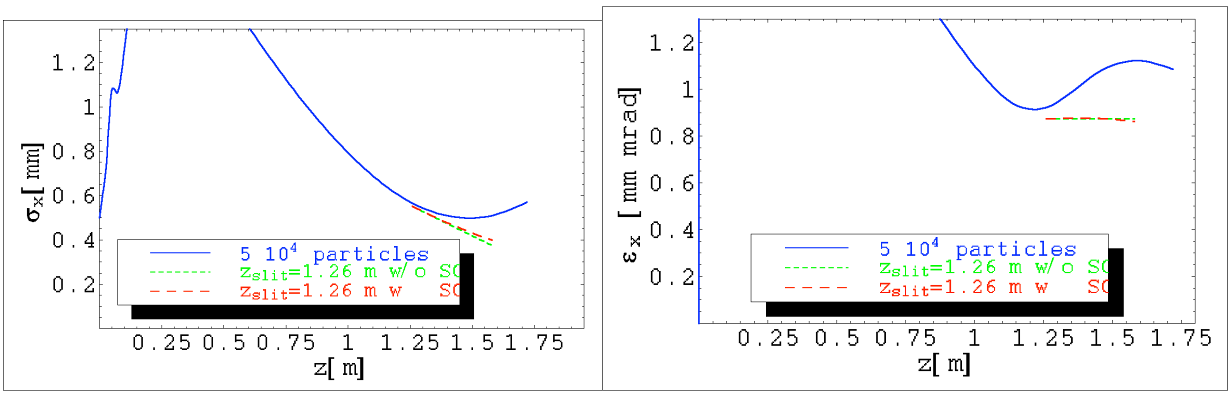

(a) **(b)**

Figure 23 (a) envelope (σ_x) and (b) emittance (ε_x) with and without space charge effects. The solid line refers to the whole beam. The slit is at z=1.26 from the cathode.

When considering the differences between the beam entering the multi-slit device and the one just emerging from it, one observes that in the first case the envelope is not modified appreciably by the cut, while the emittance is slightly diminished. At the waist, by contrast, the emittance is slightly increased and also the envelope is affected, mainly because of the reduced number of beamlets. It is worth remarking that these quantities refer to the numerical "truth" reported by the simulation code, not to the distortion introduced by the measurement procedure.

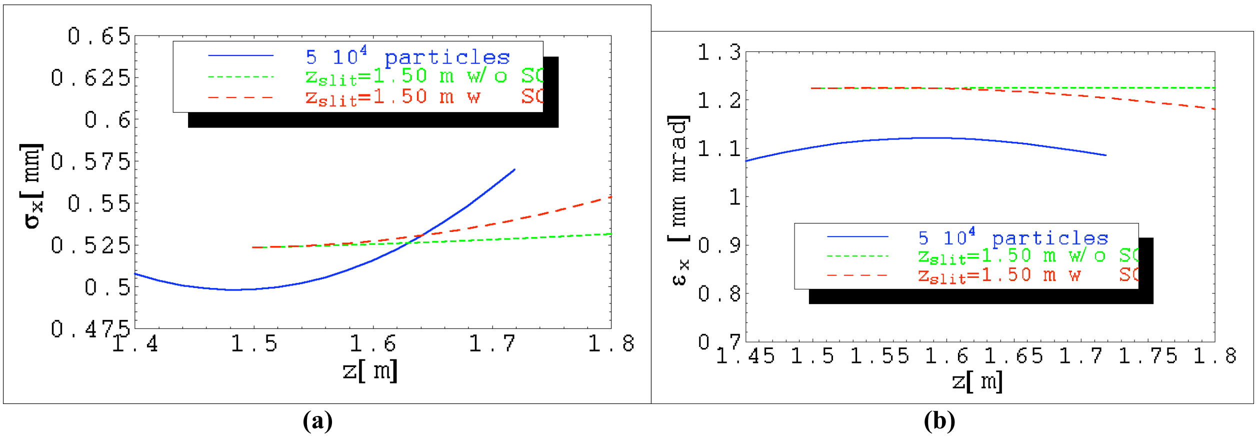

Figure 24: Same as above. The slit is at z=1.50m from the cathode (the envelope waist). Only the region around the position of the multi-slit device is shown.

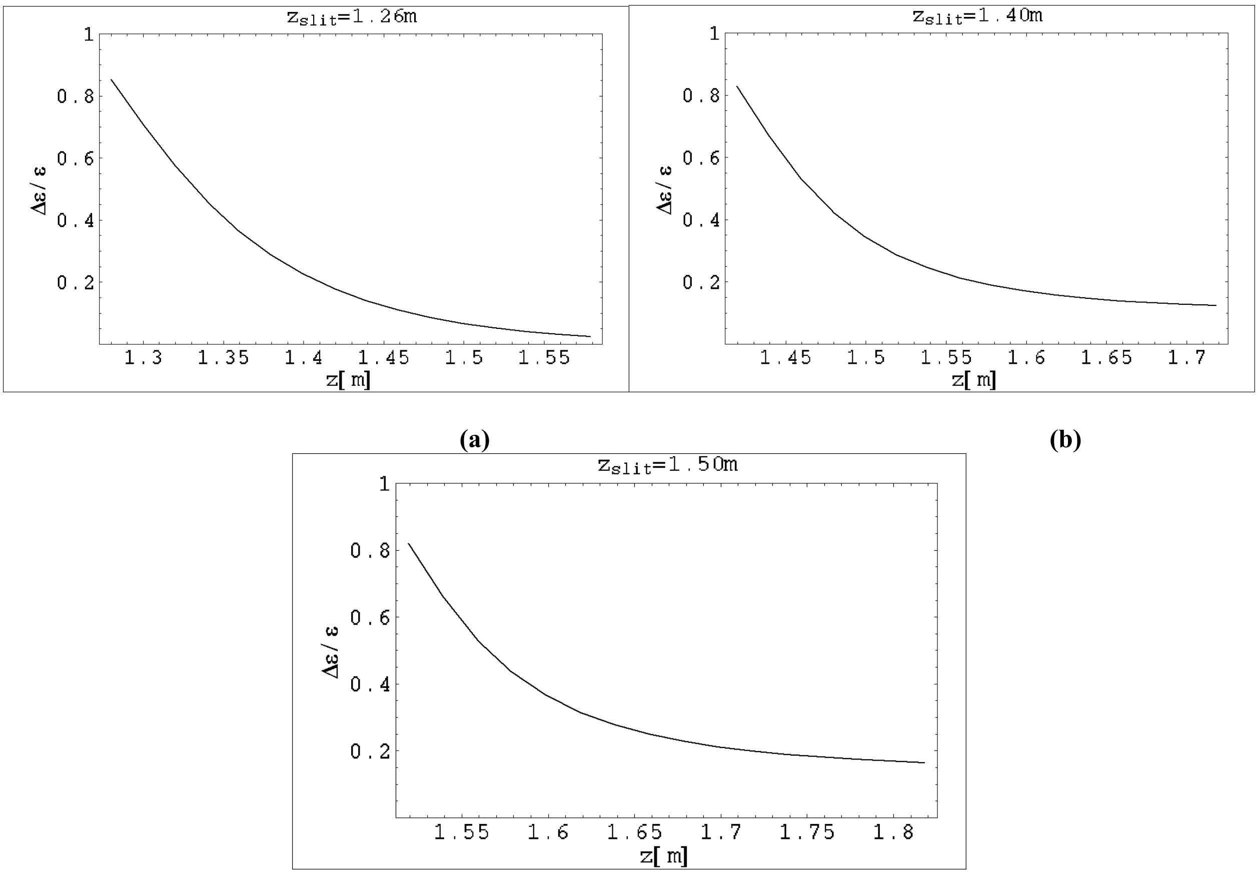

(c)

Figure 25: Relative error in emittance reconstruction as a function of the distance of the screen from the multi-slit. From top to bottom, left to right slit position at z=1.26m z=1.40 and z=1.50m, respectively.

On the other hand, the differences are not numerical artifacts of the simulation itself, since one is looking at the beamlets immediately after the cut, when no transport has been simulated yet. In other words it must be clear that what is being measured is the emittance of the beamlets ensemble (the beam *after* the cut), which may well *not be* an accurate estimation of the quantity one is really willing to evaluate (the emittance of the beam *before* the cut). The discrepancies are essentially due to the combination of a purely *geometric* effect (the multi-slit cut) and, as will be made clear below, to the accuracy achievable in describing the details of the transverse 4D phase space. The uncertainty in the latter is indeed the only source of error for the effect of the cut can be precisely estimated and for this reason should not be considered really as an error as long it can be assumed that the numerical phase space impinging on the multi-slit device yields a faithfully description of the beam in the real case. Then, at least in principle, form the simulations one can compute a correction factor to be applied to the results of the measurement to take into account the distortion produced by the cut. As it will be clear in the following (see fig. 26) , the accuracy of the measurement is subject to large oscillations, due to the the fact that the quantities entering the Zhang formula for emittance evaluation are affected by the cut in a complicated fashion. For this reason, in the analysis described below, the results will be presented without this factor, which will be discussed thoroughly in a forthcoming note. For simplicity, in the measurement simulation the quantities entering the Zhang formula have been evaluated assuming perfect assignment of particles to the beamlets, which is clearly not the situation one faces experimentally. This means that results do not include the error in reconstructing the cumulative charge, average positions and r.m.s widths of the beamlets on the CCD screen due to beamlets overlapping, quantization errors and finite resolution effects. In fig. 25 the error in the emittance reconstruction is shown as a function of the distance between the screen and the multi-slit for three different positions. In fig. 26 the relative error as a function of the position of the slit is shown. Large oscillations are visible, suggesting that the quantities entering the emittance formula are affected in a complicated fashion by the multi-slit selection..

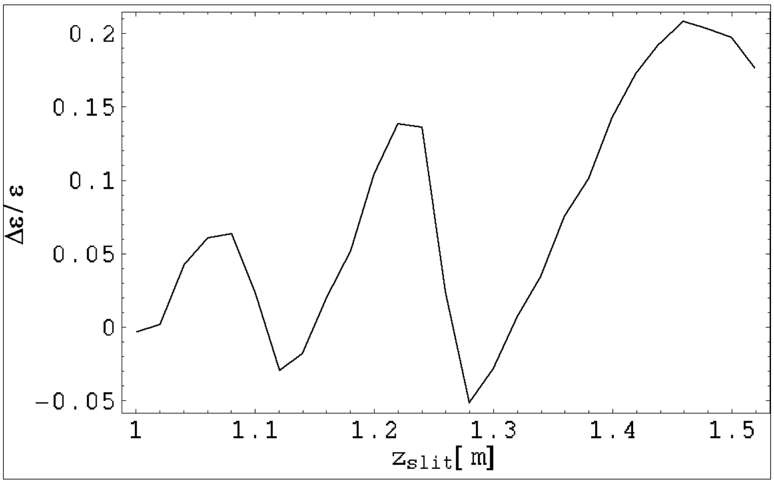

Figure 26:. Relative error in emittance estimation as a function of the slit plate. The large oscillation are due to the subtle interplay of the distortions affecting the quantities entering the emittance formula produced by the cut.

As a final note, it is worth remarking that the “hollow beam” effect observed in PARMELA has been confirmed in the TREDI simulations. In fig. 27 is shown the $\square^2$ distribution for the particle of the beam at z=1.26m, z=1.40 and z=1.50 m. The histograms are supposed to be flat for a cylindrical beam of homogeneous density, but in the case of the waist clearly show an excess of particles at the border of the beam, not observed at the other two positions. The higher density seems to be concentrated in the central longitudinal slices, as is clearly visible in the fig. 28, where the x-y space for the central slice (out of 9) is shown. This effect is visible in the plot of radial field (fig 29) for the same slice, which grows up more rapidly at the border.

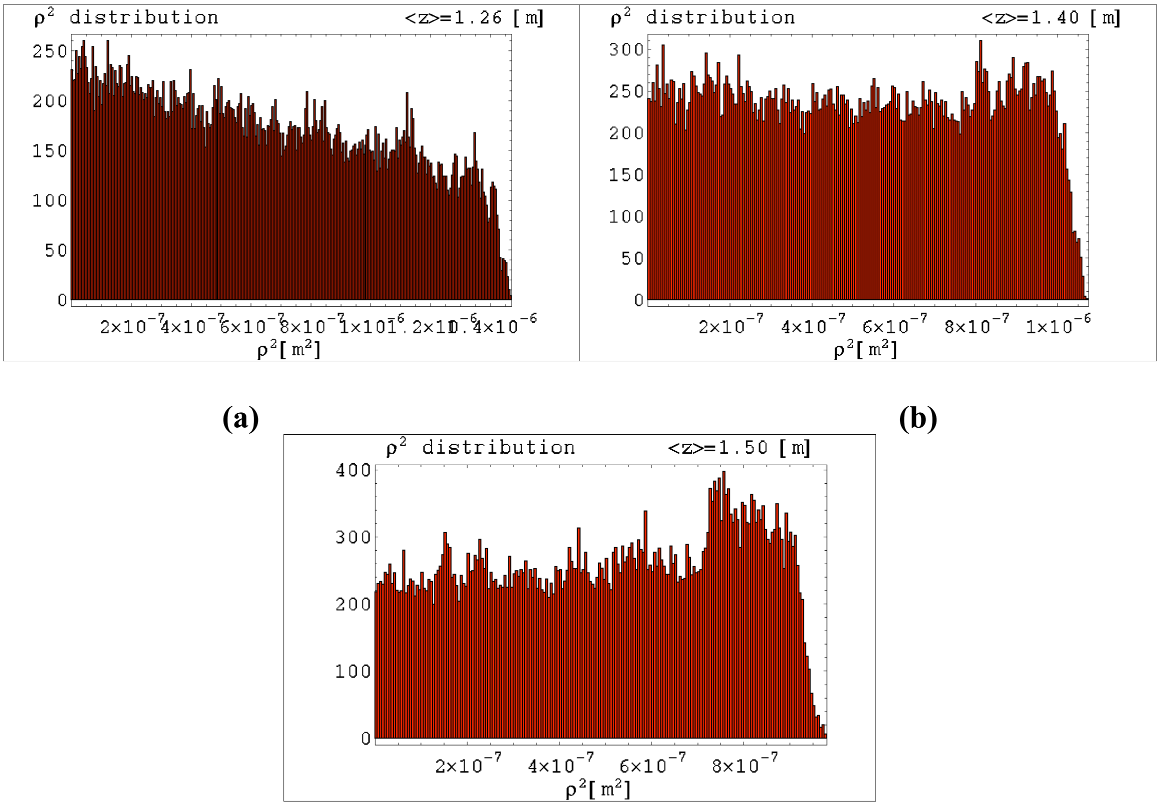

(a) **(b)**

(c)

Figure 27: Density plot of ρ^2 at the waist.

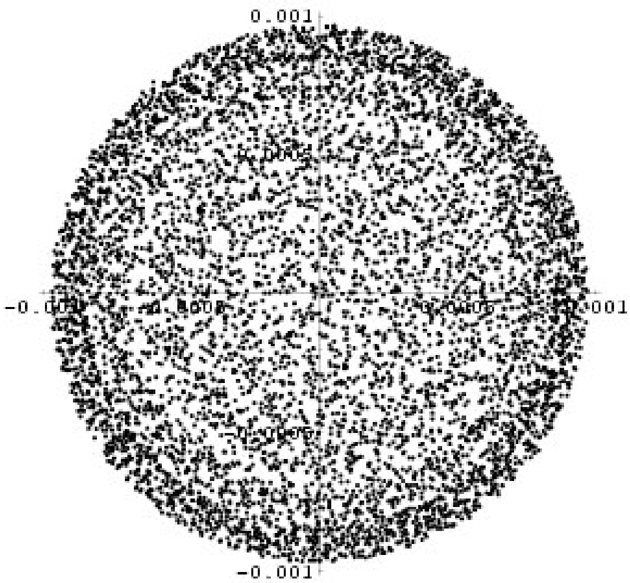

Figure 28:. x-y space for the slice 5 out of 9 at z=1.50 m. Note the higher density at the border.

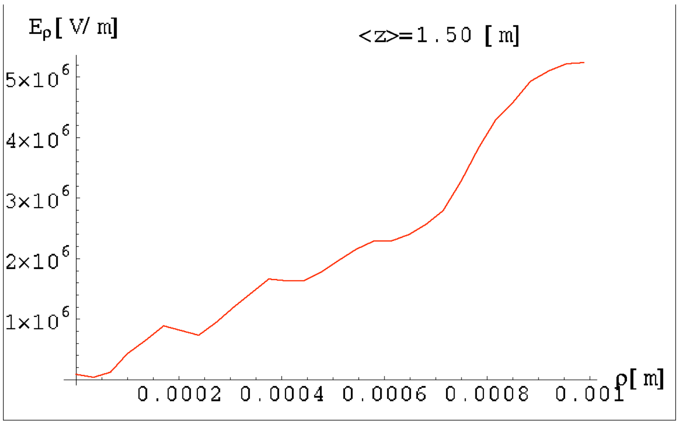

Figure 29:. Radial (space charge) electric field as a function of the distance from the longitudinal axis. Note the increased slope at the border, reflecting the higher charge density.

10 CONCLUSIONS

The simulation results of the emittance measurement give some useful indications in order to optimally design a slit-based trace space measurement system. As it is summarized in table 2, due to the different beam conditions in the emittance compensation process region different designs could be necessary in order to minimize the error in the retrieved parameters over the required longitudinal range.

TABLE 2

	Region extension (approximate)*	**Best method**	**Geometrical parameters ****
Beam converging region	85-120 cm	Two shots multislit Or Multishot scanning single slit	d=50 μm, d+w=500 μm, L=20 cm d=50 μm, scanning step=250 μm
Waist region	120-160 cm	Two shots Multislit Or Multishot scanning single slit	d=50 μm, d+w=500 μm, L=20-30 cm d=50 μm, scanning step=100-250 μm
Beam diverging region	160-200 cm	Single shot Multislit	d=50 μm, d+w=500 μm, L=40 cm

*z=0 at the cathode, ** d=slit width, w=interslit distance,L=distance between slits and output screen

According to our simulation results for an initial uniform radial distribution and different longitudinal positions it seems that in the conditions reported in table 2 it is possible to achieve a maximum relative error on emittance of the order of 10%.
However this consideration is based on an ideal situations without noise and the use of an analysis program that is able to resolve with sufficient accuracy the output intensity distribution.

In a “real” measure, when the multislit technique is used, the simplified algorithm that we employed for this evaluation that is able to separate the peaks identifying the minima between the peaks could be not applicable due to the measure noise. In practice in order to handle noisy data and to resolve partially overlapping peaks the standard acquisition programs use a gaussian fit of the slit image, but probably for SPARC in some places this method is not directly applicable for the mutlislit technique.
In fact the intensity profile of the single beamlets (expecially in the tails) is not everywhere a simple Gaussian or other well-defined singly peaked distribution. This feature complicates the analysis of the slit-collimated beam images. A detailed reconstruction of the distribution seems not to be possible with a simple rms beamlet width analysis, but a fit based on a sum of Gaussians [4] or other analysis methods could be necessary.
We want to remark that in addition to the “standard” method described in this note based on the use of the formula reported in appendix 1 other methods for evaluating the rms emittance can be employed as it has been done in PITZ (Photo Injector Test Facility at Desy Zeuthen) where other two alternative methods were used [5,6]: the first method consists in measuring directly the beam rms size at the position of the slit mask and obtaining the divergence and covariance of the transverse phase space distribution by the analysis of the beamlet profiles as in the method described here; the second method consists in evaluating the emittance as a product of the measured rms beam size and the weighted average of the rms divergence of the different beamlets.

11 REFERENCES

[1] M. Zhang “Emittance Formula for Slits and Pepper-pot measurement”, FERMILAB-TM-1998
[2] Anderson, J.B. Rosenzweig et al. “ Space-charge effects in high brightness electron beam emittance measurements”, Phys. Rev. Special Topics – Acc. and beams, Volume 5, 014201 (2001)
[3] J. G. Power “Slit scattering effects in a well aligned pepper pot”, PAC 2003
[4] Dolinska et al. “Emittance measurements at the new UNILAC pre-stripper using a pepper-pot with a pc-controlled ccd-camera“ DIPAC ‘99
[5] R. Bakker et al. “ First measurements at the photoinjector test facility at DESY Zeuthen”, Proceedings EPAC 2002, Paris, France, pag. 1813
[6] K. Abrahamyan et al. “ Transverse emittance measurements at the phgotoinjector test facility at DESY Zeuthen (PITZ) “, Proceedings DIPAC 2003 –GSI, Mainz, Germany

APPENDIX 1: EMITTANCE FORMULAS FOR SLITS MEASUREMENT (from ref. [1])

$$\varepsilon^2{}_x \approx \frac{1}{N^2}\left\{\left[\sum_{j=1}^{p} n_j (x_{sj}-\overline{x})^2\right]\left[\sum_{j=1}^{p}\left[n_j \sigma_{x'_j}{}^2 + n_j(\overline{x'_j}-\overline{x'})^2\right]\right]-\left[\sum_{j=1}^{p} n_j x_{sj} x'_j - N\overline{x}\overline{x'}\right]^2\right\}$$

where

x_{sj} : j-th slit's position;
P: total number of slits;
n_j : number of particles passing through j-th slit and hitting the screen. This is a practical weighting of spot intensity;
$\overline{x}$: mean position of all beamlets;
x'_j : mean divergence of j-th beamlet;
$\overline{x'}$: mean divergence of all beamlets;
$\sigma_{x'_j}$: rms divergence of j-th beamlet.

APPENDIX 2: SLIT DESIGN CRITERIA

Following the treatment of ref. [2] which describes the design criteria and the physical principles involved in phase space measurement based on collimating slits, in this section the analytical formulas for a preliminary design of a slit-based emittance meter are collected. The analysis has been done in the waist.
From the RMS envelope equation in a drift space that is

$$\sigma_x'' = \frac{\varepsilon_n^2}{\gamma^2 \sigma_x^3} + \frac{4I}{\gamma^3 I_0(\sigma_x + \sigma_y)}$$

the ratio of the space charge to the emittance term before the beam goes through the slits is

$$R_0 = \frac{2I\sigma_0^2}{I_0 \gamma \varepsilon_n^2},$$

that for **I=100 A, σ_0=0.5 mm, ε_n= 1 mm mrad** gives ***R_0*=245.94** (Space charge dominated regime)

Noting that the rms size of a uniform beamlet created by a vertical slit of width d is $\sigma_x = d/\sqrt{12}$ and assuming $\sigma_x >> \sigma_y$, after the beam goes through the slits the ratio of the space charge term to the emittance term in the beamlet rms envelope equation becomes

$$R_b = \sqrt{\frac{2}{3\pi}}\,\frac{I}{\gamma I_0}\left(\frac{d}{\varepsilon_n}\right)^2$$

that for ***d* □ 66□m gives *R_b* □ 1**, that means that 66 □m is the maximum tolerable slit width. **For *d* □ 50□m *R_b* = 0.566**

The beam rms angle at a waist is given by

$$\phi = \frac{\varepsilon_n}{\gamma\sigma_0}$$

the ratio of this angle to slit acceptance □***L*/*d*** (*L*=slit depth) should be less than 1. In our case it is **6.7 10^{-3}** in the waist.

The slit separation w is chosen to be much larger than the slit width and smaller than rms beam size, to ensure that the beam can be resolved:

$$d << w < \sigma_0$$

The ratio between the beamlet widths to the their separation

$$R_{ws} = 2\frac{L_d\phi}{w}$$

should be much smaller than 1 in order to avoid overlapping, while the ratio of the beamlet rms size at the output screen to its size at the slit:

$$R_{sp} = 2\sqrt{3}\,\frac{L_d\phi}{d}$$

should be much larger than unity in order to achieve resolution of the angular spread.
Since one of this ratios should be smaller and the other larger compared to unity, if we set their geometric average equal to unity ($R_{ws} \cdot R_{sp}$ =1) the optimum drift length to output screen is

$$L_d = \frac{\sqrt{dw}}{3^{1/4}\,2\phi}$$

that for our parameters gives **L_d=34 cm** corresponding to **R_{ws}=0.253 and R_{sp}=3.939**.

Accordingly with the Courant theory, the minimum signal-to-noise due to the slit-scattering for the detected beam-intensity at the output screen is

$$\frac{S}{N} \geq \frac{\sqrt{3\pi}\,dw_c}{2d_{eff}L_{eff}^{3/2}}$$

where

$$L_{\text{eff}} = L_r \left(\frac{21 \cdot d}{E[MeV] \cdot 2L} \right)^2$$

$$d_{\text{eff}} = \frac{2}{\sqrt{3\pi}} \frac{L_{\text{eff}}^{3/2}}{w_c}$$

$$w_c^2 = \frac{A}{Z^2 \pi N_A \rho} \left(\frac{E}{2e^2} \right)^2 \frac{1}{\ln\left(181 \cdot Z^{1/3}\right)}$$

giving minimum *S/N*=83.

Table A2.1 and table A2.2 respectively summarize the parameters and the relative figures of merit deriving from these formulas for SPARC

TABLE A2.1. Slit measurement system design parameters

Parameter	**Value**
Beam current	100 A
Beam rms normalized emittance	1 mm mrad
Beam initial size □$_0$	0.5 mm
Slit width *d*	<66 □
Slit separation *w*	450 □
Slit depth *L*	2 mm

TABLE A2.2. **Figures of merit for d=50 □m**

Parameter	**Value**
Beam space charge ratio $\boldsymbol{R_0}$	□246
Beamlet space charge ratio $\boldsymbol{R_b}$	0.566
Optimal drift length $\boldsymbol{L_d}$	34 cm
Signal to noise ratio ***S/N***	83